Deliquescence of $NaCl–NaNO_3$, $KNO_3–NaNO_3$, and $NaCl–KNO_3$ salt mixtures from 90 to 120 °C

Susan Carroll,[a] Laura Craig, and Thomas J. Wolery
Energy and Environment Directorate, Lawrence Livermore National Laboratory, Livermore, California 94550

(Received 11 November 2004; accepted 26 January 2005; published online 11 April 2005)

We conducted reversed deliquescence experiments in saturated $NaCl–NaNO_3–H_2O$, $KNO_3–NaNO_3–H_2O$, and $NaCl–KNO_3–H_2O$ systems from 90 to 120 °C as a function of relative humidity and solution composition. NaCl, $NaNO_3$, and KNO_3 represent members of dust salt assemblages that are likely to deliquesce and form concentrated brines on high-level radioactive waste package surfaces in a repository environment at Yucca Mountain, NV. Discrepancy between model prediction and experiment can be as high as 8% for relative humidity and 50% for dissolved ion concentration. The discrepancy is attributed primarily to the use of 25 °C models for $Cl–NO_3$ and $K–NO_3$ ion interactions in the current Yucca Mountain Project high-temperature Pitzer model to describe the nonideal behavior of these highly concentrated solutions. © *2005 American Institute of Physics.* [DOI: 10.1063/1.1872292]

I. INTRODUCTION

Yucca Mountain, NV is the designated geologic repository for permanent disposal of high-level nuclear waste. Current waste package design calls for double walled containers with an inner wall of stainless steel and an outer wall of highly corrosion resistant Ni–Cr–Mo alloy, which are protected with Ti shields to prevent rocks and seepage water from contacting the containers.[1] Of concern are the corrosion resistance and long-term integrity of these metal barriers. If the Yucca Mountain site license is approved, the waste packages will be placed in tunnels several hundred meters below the ground surface in partially saturated volcanic tuff, but still well above the groundwater table. A likely source of brines that may potentially corrode metal containers and drip shields are those formed by the absorption of water by hygroscopic salts found in local and regional dust deposited during repository construction and ventilation stages.

Accurate prediction of brine formation is important for the safe disposal of radioactive waste, because brine composition is an indicator of the corrosiveness of the aqueous environment and the relationship between deliquescence relative humidity and temperature is an indicator of ''repository dryness.'' Deliquescence refers to the formation of an aqueous solution by the absorption of water by hygroscopic salt minerals. This process allows brines to form above 100 °C at standard atmospheric pressure of 1.013 25 bar (or above 96 °C and 0.9 bar at the repository elevation of 1039–1107 m; BSC, 2004a, Sec. 6.7.2.1). The relative humidity at which salts deliquesce is dependent on temperature and is characteristic to each salt mineral or assemblage of salt minerals. For example at 90 °C, $MgCl_2$ deliquesces at 24% relative humidity and KCl deliquesces at 78.5% relative humidity.[2] Generally, the deliquescence relative humidity for a salt mixture is lower than the deliquescence relative humidity for its pure salt components. Salt deliquescence data are largely limited to 25 °C for mixed salts[3–5] but are widely available for single salts at higher temperatures.[2]

The range of brines formed by the deliquescence of hygroscopic salts found in dusts can be calculated from mixtures of the pure phases using equilibrium thermodynamics, because relative humidity is related to the activity of water and solution composition. Wolery and Wang[6] used the EQ3/6 geochemical code and the Yucca Mountain Project high-temperature Pitzer model to predict the deliquescence of salt mixtures found in Yucca Mountain dust samples collected from exploratory tunnels. The modeling results predict that mixtures of NaCl, KNO_3, and/or $NaNO_3$ are the most prevalent mineral assemblages, and that inclusion of KNO_3(s) lowers the deliquescence relative humidity from values near 70% at 25 °C to values as low as 20% at 160 °C. This analysis implies that concentrated brines may contact the metal container and drip shield surfaces at low relative humidity and high temperature.

In this paper we compare model predictions and experimental results of relative humidity and solution compositions for saturated $NaCl–NaNO_3–H_2O$, $KNO_3–NaNO_3–H_2O$, and $NaCl–KNO_3–H_2O$ systems from 90 to 120 °C. These are benchmark experiments that can be used to assess the validity of the model calculations and Pitzer parameters that account for nonideal ion interactions in these highly concentrated solutions.

II. MODEL CALCULATIONS

Relative humidity is thermodynamically tied to solution composition through the activity of water. For water, its activity, a_w, is the product of its mole fraction, x_w, and its mole fraction activity coefficient, γ_w:

$$a_w = x_w \gamma_w . \tag{1}$$

The mole fraction of water is dependent on the solution composition:

[a]Author to whom correspondence should be addressed; electronic mail: carroll6@llnl.gov

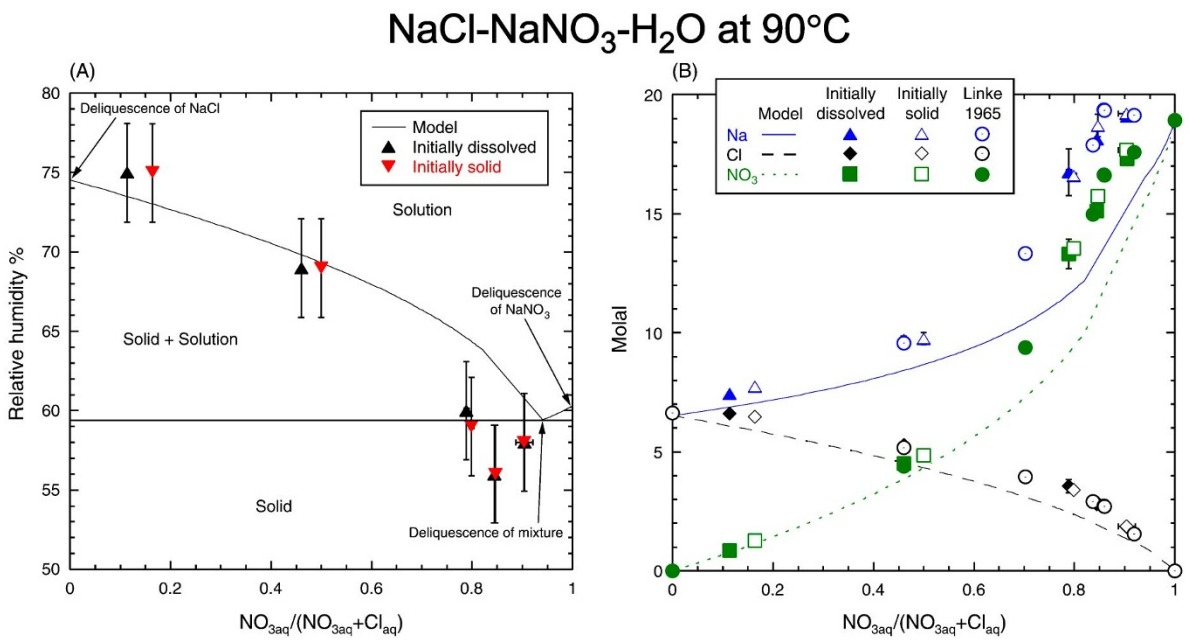

FIG. 1. (Color) Deliquescence of NaCl–$NaNO_3$ salts at 90 °C starting from initially dissolved and initially solid mixtures plotted as (a) % relative humidity and (b) solution composition.

$$x_w = n_w \Big/ \left(n_w + \sum_i n_i \right) \tag{2}$$

where n_w and n_i are the number of moles of water and of dissolved ionic constituent i, respectively. The concentrations of the dissolved constituents are limited by the solubilities of the thermodynamically stable salt minerals. If we use halite (NaCl) as an example, then the solubility product, K_{NaCl}, at a given temperature is dependent on the Na^+ and Cl^- concentrations and activity coefficients according to the mass balance reaction:

$$\mathrm{NaCl(s)} = \mathrm{Na^+ + Cl^+}, \tag{3a}$$

$$K_{\mathrm{NaCl}} = (m_{\mathrm{Na^+}} \gamma_{\mathrm{Na^+}})(m_{\mathrm{Cl^-}} \gamma_{\mathrm{Cl^-}}), \tag{3b}$$

where m_i and γ_i indicate the molality and activity coefficient of species i, with unit activity implied for the solid (NaCl).

Relative humidity, $\mathrm{RH_{frac}}$, is related to activity of water through the partial pressure of water vapor, and is equivalent to

$$\mathrm{RH_{frac}} = p_w / p_w^0, \tag{4}$$

where p_w is the partial pressure of water vapor over an aqueous solution and p_w^0 is the partial pressure of water vapor over pure water. Similarly, the activity of water is equivalent to

$$a_w = f_w / f_w^0, \tag{5}$$

where f_w is the fugacity of water vapor over an aqueous solution and f_w^0 is the fugacity of water vapor over pure water. Equating fugacity with its partial pressure:

$$f_w / f_w^0 = p_w / p_w^0 \tag{6}$$

yields:

$$\mathrm{RH_{frac}} = a_w. \tag{7}$$

The activity of water is commonly expressed in decimal form and RH is commonly expressed as a percentage; thus $\mathrm{RH\%} = 100 \times a_w$.

In hydrologically unsaturated environments, the partial pressure of water cannot exceed the total pressure. The partial pressure of water is related to the vapor pressure of pure water and the activity of water by $p_w = p_w^0 a_w$. Both the vapor pressure of pure water and the partial pressure of water over a salt solution increase strongly with temperature above 100 °C. Brines cannot exist at temperatures above the dry-out temperature, where the partial pressure of water equals the total pressure. Above the dry-out temperature only solid salt minerals and water vapor occur. Since this process is reversible, the dry-out temperature is also the deliquescence temperature for the same assemblage of salt minerals (note: at much lower temperature, generally 25 °C or less, dry-out or ''efflorescence'' is controlled by salt mineral nucleation instead of equilibrium thermodynamics.[5] The deliquescence temperature is also equivalent to the boiling point for the saturated solution.

Brines formed by the absorption of water by deliquescent minerals are thermodynamically equivalent to brines that are saturated with respect to the same deliquescent minerals. Figures 1–5 show the model calculations of relative humidity and solution composition from 90 to 120 °C versus X_{NO3} or X_{Na} for the NaCl–$NaNO_3$–H_2O, the KNO_3–$NaNO_3$–H_2O, and the NaCl–KNO_3–H_2O systems. For the NaCl–$NaNO_3$–H_2O system, this is done by adding soda niter ($NaNO_3$) to a halite (NaCl) saturated solution until the solution is saturated with both soda niter and halite. This represents the eutonic point for the NaCl–$NaNO_3$ salt assemblage. The calculation for this assemblage is completed by a complementary run in which halite is added to a soda niter saturated solution until the same eutonic point is

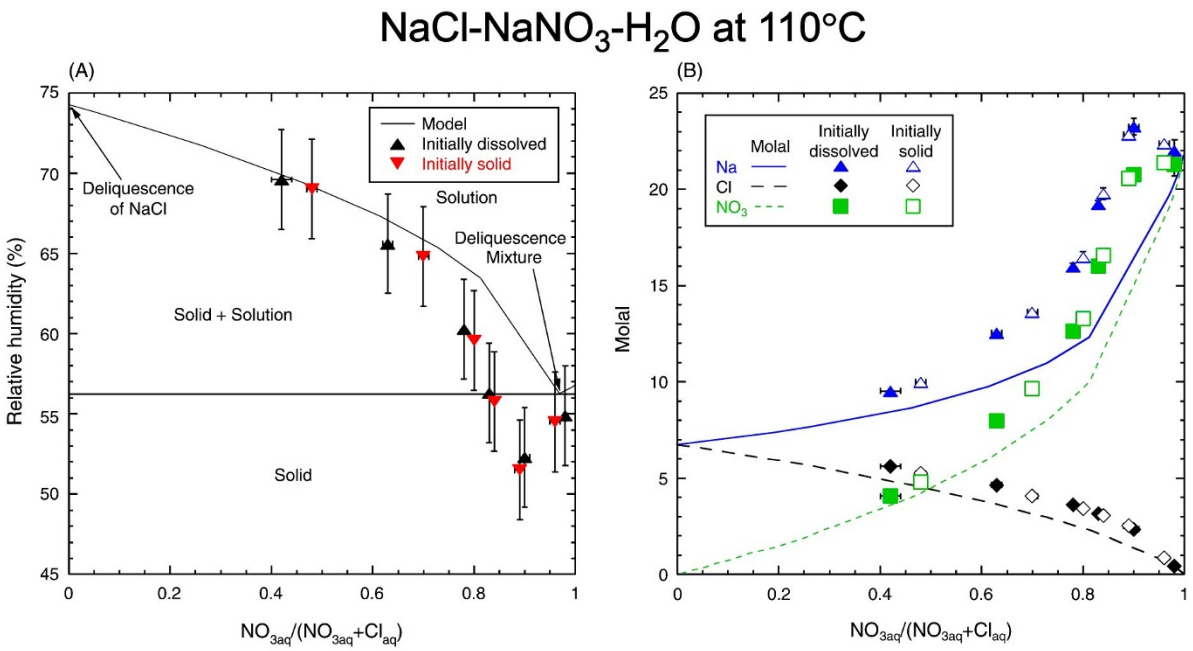

FIG. 2. (Color) Deliquescence of NaCl–$NaNO_3$ salts at 110 °C starting from initially dissolved and initially solid mixtures plotted as (a) % relative humidity and (b) solution composition.

reached. An identical approach is used for the $KNO_3-NaNO_3-H_2O$ and $NaCl-KNO_3-H_2O$ systems. We use the EQ3/6 geochemical code[7] and the Yucca Mountain Project high-temperature Pitzer model.[8] This model is based on the Pitzer equations (cf. Ref. 9) to account for the non-ideal behavior of the brine solutions. Reaction pressure was allowed to vary by means of the 1.013 bar/steam-saturation curve. The Pitzer model is based on the available experimental data and includes binary interactions $(\beta^{(0)}_{M,X}, \beta^{(1)}_{M,X}, \beta^{(2)}_{M,X}, C^{\phi}_{M,X})$ between two different kinds of ions of opposite charge (cation M and anion X), and also binary $(\theta_{M,M'}, \theta_{X,X'})$ interactions between ions of like charge and ternary interactions $(\psi_{M,M',X}, \psi_{X,X',M})$ involving three ions in common-cation and common-anion ternary systems. Pitzer parameters relevant to this study are listed in Table I.

III. EXPERIMENTAL METHODS

A. Starting materials

Analytical grade sodium chloride (NaCl, 100.1% pure), sodium nitrate ($NaNO_3$, 99.7% pure), and potassium nitrate (KNO_3, 99.5% pure) were used to synthesize dissolved and dry salt mixtures. Impurities in NaCl include less than 0.01%

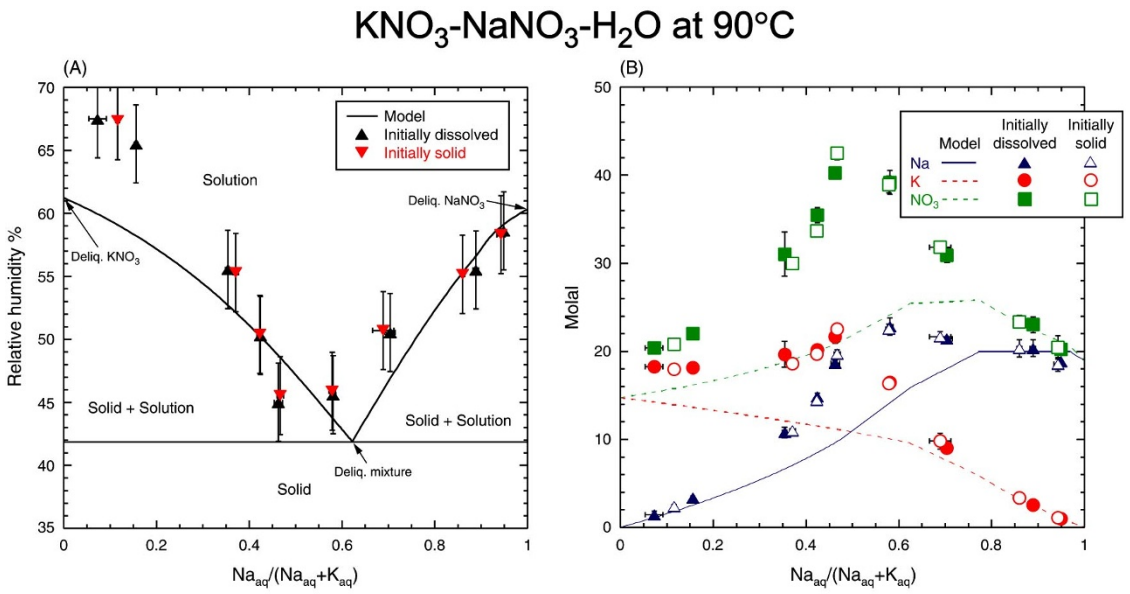

FIG. 3. (Color) Deliquescence of KNO_3-NaNO_3 salts at 90 °C starting from initially dissolved and initially solid mixtures plotted as (a) % relative humidity and (b) solution composition.

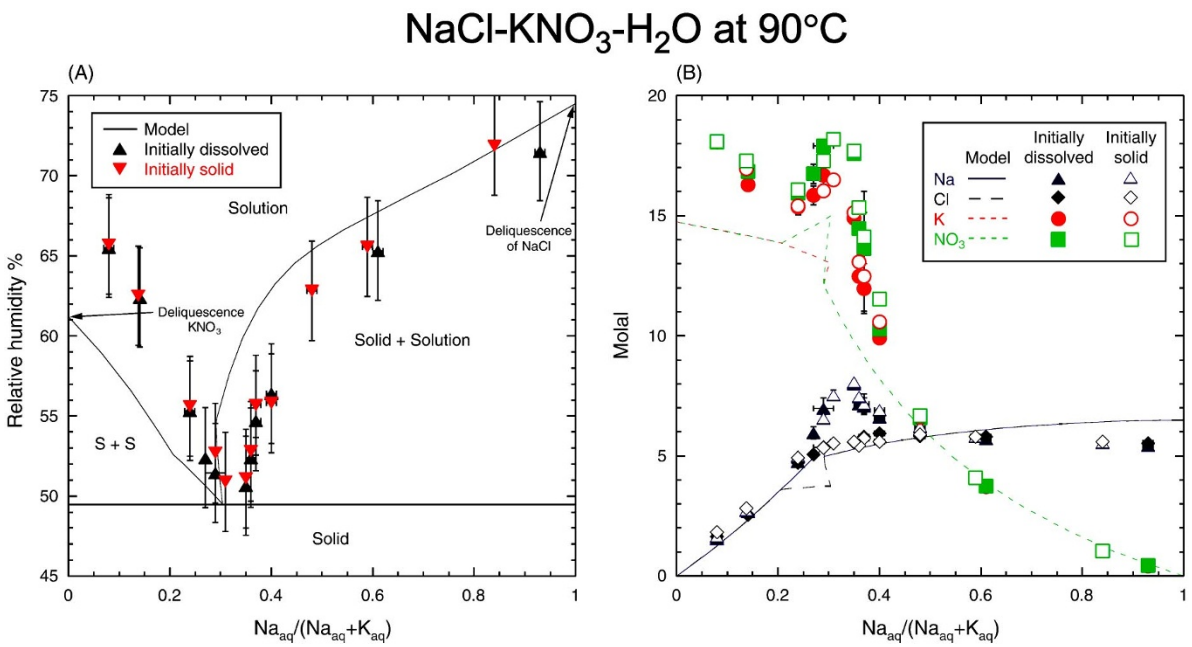

FIG. 4. (Color) Deliquescence of NaCl–KNO_3 salts at 90 °C starting from initially dissolved and initially solid mixtures plotted as (a) % relative humidity and (b) solution composition.

Br; 0.005% K; 0.004% SO_4, 0.003% ClO_4, NO_3, and Ba; 0.002% I and Ca; 0.001% Mg; 5 ppm PO_4; 2 ppm heavy metals, and 1 ppm Fe. Impurities in $NaNO_3$ include less than 0.002% K; 0.001% SO_4, NO_2, Ca, Mg, and R_2O_3; 0.0005% Cl; 3 ppm PO_4 and heavy metals, and 1 ppm Fe and IO_3. Impurities in KNO_3 include less than 0.004% Na; 0.002% SO4; 0.001% Cl, and NO_2, 0.0005% Ca; 0.0002% Mg; 3 ppm heavy metals, 2 ppm PO_4; and 1 ppm Fe and IO_3. Distilled and de-ionized (18 M Ω) water was used to make all solutions.

B. Reverse deliquescence experiments

We measured brine composition at controlled relative humidity for NaCl–$NaNO_3$, KNO_3–$NaNO_3$, and NaCl–KNO_3 salt mixtures from 90 to 120 °C as a function of X_{NO3} or X_{Na}. Our experimental design mimics the model calculations in that one salt in the binary system will completely dissolve and the dissolution of the other will be limited by its solubility. We approached the equilibrium brine composition by placing identical mole fractions of dissolved

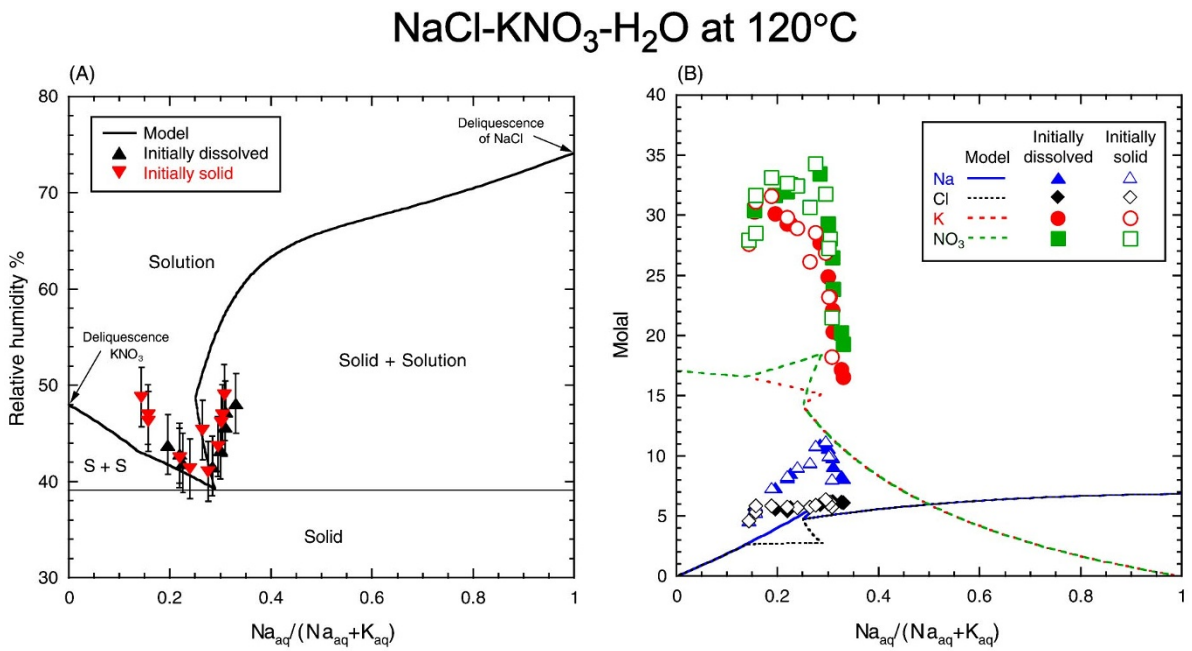

FIG. 5. (Color) Deliquescence of NaCl–KNO_3 salts at 120 °C starting from initially dissolved and initially solid mixtures plotted as (a) % relative humidity and (b) solution composition.

TABLE I. Pitzer interaction parameters used with EQ3/6 to calculate relative humidity and solution composition in saturated brines containing Na, K, Cl, and NO_3. Temperature dependence of each of these ion interaction parameters is derived from Eq. (11): $\chi(T)=a_1+a_2/(T-T_r)+a_3\ln(T/T_r)+a_4(T-T_r)$.

Ion interactions	Coefficients	Pitzer interaction parameters a_1	a_2	a_3	a_4	Reference
K–Cl	$\beta^{(0)}_{MX}$	4.78×10^{-02}	$-3.43\times10^{+02}$	-1.38	1.34×10^{-03}	10
	$\beta^{(1)}_{MX}$	2.16×10^{-01}	$-5.76\times10^{+02}$	-2.88	4.64×10^{-03}	
	$\beta^{(2)}_{MX}$	0.00				
	C^{ϕ}_{MX}	-7.49×10^{-04}	$3.65\times10^{+01}$	1.48×10^{-01}	-1.47×10^{-04}	
K–NO_3	$\beta^{(0)}_{MX}$	-8.16×10^{-02}				9
	$\beta^{(1)}_{MX}$	4.94×10^{-02}				
	$\beta^{(2)}_{MX}$	0.00				
	C^{ϕ}_{MX}	6.60×10^{-03}				
Na–Cl	$\beta^{(0)}_{MX}$	7.46×10^{-02}	$-4.71\times10^{+02}$	-1.85	1.66×10^{-03}	10
	$\beta^{(1)}_{MX}$	2.75×10^{-01}	$-5.21\times10^{+02}$	-2.88	4.71×10^{-03}	
	$\beta^{(2)}_{MX}$	0.00				
	C^{ϕ}_{MX}	1.54×10^{-03}	$4.81\times10^{+01}$	1.75×10^{-01}	-1.56×10^{-04}	
Na–NO_3	$\beta^{(0)}_{MX}$	3.57×10^{-03}	$-7.03\times10^{+02}$	-3.35	3.98×10^{-03}	11
	$\beta^{(1)}_{MX}$	2.32×10^{-01}	$-2.73\times10^{+03}$	$-1.30\times10^{+01}$	2.07×10^{-02}	
	$\beta^{(2)}_{MX}$	0.00				
	C^{ϕ}_{MX}	-4.15×10^{-05}	$6.48\times10^{+01}$	3.18×10^{-01}	-3.84×10^{-04}	
K–Na	${}^{S}\theta_{MM'}$	-3.20×10^{-03}	$1.40\times10^{+01}$	9.09×10^{-13}	-2.66×10^{-15}	10
Cl–NO_3	${}^{S}\theta_{XX'}$	1.60×10^{-02}				9
K–Na–Cl	$\psi_{MM'X}$	-3.69×10^{-03}	-5.10	-3.41×10^{-13}	6.66×10^{-16}	10

(with about 150 g H_2O) and solid salt mixtures in an environmental chamber (Ecosphere, Despatch) at controlled relative humidity and temperature. Under these conditions the dissolved salt mixture evaporates concentrating the solution and precipitating one of the two salts, and the solid salt mixture absorbs water dissolving the salts until equilibrium is reached.

For each run, four Teflon™ beakers containing the dissolved salts and four beakers containing the solid salts were placed into the chamber and sequential pairs of initially aqueous and initially solid beakers were sampled over time. Figure 6 shows that steady-state relative humidity and solution composition are achieved with in the first 200 h of reaction and that solution composition of initially dissolved and initially solid samples converge over the time period of the experiments. Samples were typically taken every one to three days. Calibrated temperature ($\pm1°$) and relative humidity probes (Vaisala Inc., model HMP243 or HMP233) were placed just above the solutions in the beakers, because microenvironments within the beakers differed from the environmental chamber relative humidity by as much as 5% relative humidity. Relative humidity probe calibration checks were conducted in saturated KNO_3 solutions from 90 to 110 °C. Statistical analysis of these RH measurements together with vapor pressure measurements for KNO_3 (Ref. 12) yield an average standard deviation of about 1.6 RH units. Uncertainty reported in the tables and figures is calculated as 2σ (3.1% RH units).

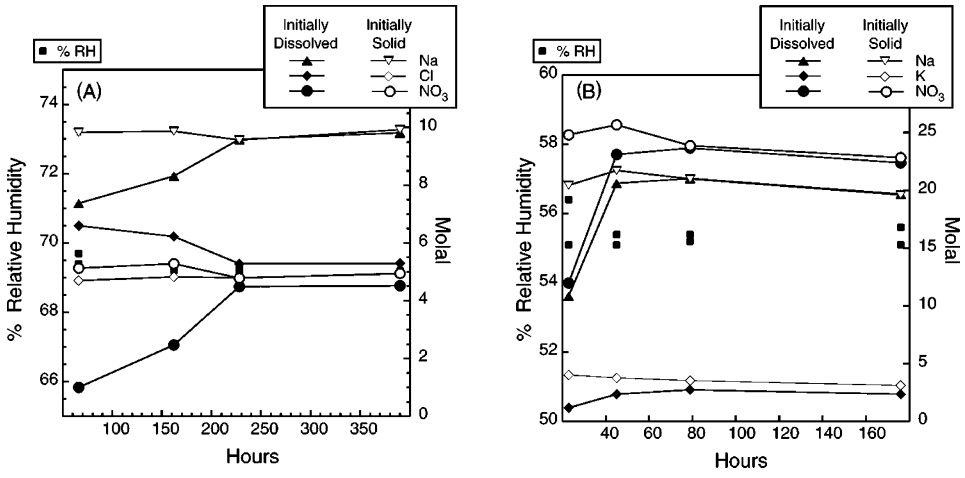

FIG. 6. Examples of the brine % relative humidity and composition as a function of time for the reversed deliquescence experiments at 90 °C for (a) NaCl–$NaNO_3$ and the (b) KNO_3–$NaNO_3$ mixtures.

TABLE II. Solution % RH and composition from reversed deliquescence of $NaCl–NaNO_3$ mixtures at 90 °C. Reported values represent the average steady-state solution composition.

Expt. ID	T (°C)	%RH ±3.1	Na molal	Cl molal	NO_3 molal	$[NO_3]/[NO_3]+[Cl]$
			Initially dissolved salt			
MS-9A	91	74.6	7.44±0.01	6.60±0.03	0.85±0.00	0.11±0.00
MS-10A	90	69.3	9.70±0.16	5.29±0.01	4.50±0.02	0.46±0.00
MS-11A	90	57.6	19.09±0.09	1.83±0.00	17.30±0.01	0.91±0.00
MS-12A	90	59.6	16.74±0.98	3.56±0.27	13.31±0.62	0.79±0.00
MS-13A	90	55.8	18.14±0.41	2.79±0.10	15.10±0.13	0.84±0.00
			Initially solid salt			
MS-9B	91	74.7	7.74±0.02	6.48±0.00	1.27±0.00	0.16±0.00
MS-10B	91	69.2	9.75±0.25	4.86±0.10	4.86±0.12	0.50±0.00
MS-11B	91	57.6	19.20±0.06	1.87±0.00	17.68±0.08	0.90±0.02
MS-12B	91	59.4	16.59±0.12	3.39±0.08	13.54±0.08	0.80±0.01
MS-13B	91	55.7	18.70±0.48	2.84±0.03	15.73±0.18	0.85±0.00

Samples were taken when there was at least 10 g of solution in each beaker. The exact amount of solution was dependent on relative humidity and solubility of the salt mixture. About 1 g of solution was collected from each beaker and filtered through a 0.45 μm syringe-less filter into a sampling bottle, the bottle was sealed and weighed to determine sample amount, and then diluted with about 250 g of distilled and de-ionized water. All dilution factors were determined gravimetrically. Each time a pair of samples was taken, the temperature and relative humidity probes were moved to monitor the next pair of beakers. Solids from the fourth pair of samples were separated from the remaining solution by filtration (0.45 μm pore size), dried, and stored in a desiccator until analyzed by powder x-ray diffraction.

C. Analytical techniques

All aqueous samples were analyzed by inductively coupled plasma-atomic emission spectrometry (ICP-AES) for sodium, and by ion chromatography (IC) for chloride, nitrate, potassium, and (for some samples) sodium. Analytical uncertainty for the ICP-AES and the IC is less than 2%. Solids were analyzed using powder x-ray diffraction for detection of halite, sylvite, soda niter, and niter. Trace amounts of a specified solid phase indicate that the intensity of major peak was generally less than 5% of the most intense peak. We suspect that the small amount of the minor component represents solution trapped during the filtration process and not an equilibrium solid.

IV. RESULTS

The deliquescence of $NaCl–NaNO_3$, $KNO_3–NaNO_3$, and $NaCl–KNO_3$ salt mixtures from 90 to 120 °C is summarized in Tables II–VI and in Figs. 1–5. Figures 1 and 2 compare the experimental results of the reversed deliquescence experiments with the model calculations for the $NaCl–NaNO_3–H_2O$ system at 90 and 110 °C. Equilibrium is shown by the convergence of the measured relative humidity and solution composition for the initially dissolved and initially solid salt mixtures. At 90 °C, we also show previous solubility data by Linke,[13] which agrees with our results.

TABLE III. Solution % RH and composition from reversed deliquescence of $NaCl–NaNO_3$ mixtures at 110 °C. Reported values represent the average steady-state solution composition.

Expt. ID	T (°C)	% RH ±3.1	Na molal	Cl molal	NO_3 molal	$[NO_3]/[NO_3]+[Cl]$
			Initially dissolved salt			
MS45-A	110	52.3	23.25±0.44	2.34±0.00	20.75±0.06	0.90±0.01
MS46-A	110	56.3	19.23±0.20	3.17±0.01	16.01±0.25	0.83±0.00
MS47-A	110	60.3	15.96±0.20	3.63±0.01	12.64±0.15	0.78±0.00
MS48-3A	110	69.6	9.53±0.01	5.62±0.00	4.07±0.02	0.42±0.02
MS49-4A	110	65.6	12.54±0.02	4.65±0.01	7.97±0.03	0.63±0.01
MS50R-A	110	54.9	22.02±0.55	0.43±0.01	21.26±0.58	0.98±0.01
			Initially solid salt			
MS45B	110	51.5	22.84±0.03	2.53±0.00	20.56±0.03	0.89±0.01
MS46-B	110	55.8	19.77±0.30	3.06±0.01	16.57±0.25	0.84±0.00
MS47-B	110	59.6	16.48±0.27	3.42±0.08	13.30±0.18	0.80±0.00
MS48-3B	110	69.0	9.99±0.00	5.25±0.01	4.79±0.01	0.48±0.01
MS49-4B	110	64.8	13.62±0.03	4.07±0.01	9.65±0.00	0.70±0.01
MS50R-B3	110	54.5	22.34±0.02	0.87±0.00	21.37±0.01	0.96±0.00

TABLE IV. Solution % RH and composition from reversed deliquescence of $NaNO_3$–KNO_3 mixtures at 90 °C. Reported values represent the average steady-state solution composition, unless otherwise noted.

Expt. ID	T (°C)	% RH ±3.1	Na molal	K molal	NO_3 molal	[Na]/ [Na]+[K]
			Initially dissolved salt			
MS-14A1	90	65.5	3.35±0.01	18.15±0.04	22.02±0.076	0.16 ±0.00
MS-14A	90	67.5	1.44±0.39	18.27±0.13	20.40±0.12	0.07 ±0.02
MS-15A	90	58.6	18.81±0.10	1.01±0.04	20.23±0.64	0.95 ±0.00
MS-16A	90	55.5	20.36±0.95	2.54±0.26	23.02±0.90	0.89 ±0.01
MS-17A	90	55.6	10.77±0.59	19.67±1.47	31.04±2.52	0.35 ±0.01
MS-18A	90	50.3	14.84±0.41	20.16±0.36	35.47±0.86	0.42 ±0.00
MS-19A	90	50.6	21.40±0.26	9.00±0.50	30.89±0.80	0.70 ±0.01
MS-20A	90	45.0	18.67±0.27	21.65±0.72	40.24±0.68	0.46 ±0.01
MS-21A	90	45.6	22.82±0.98	16.43±0.42	39.17±1.36	0.58 ±0.01
			Initially solid salt			
MS-14B	90	67.4	2.36±0.17	17.93±0.63	20.82±0.63	0.116±0.00
MS-15B	90	58.3	18.53±0.79	1.12±0.23	20.47±1.32	0.943±0.01
MS-16B	90	55.2	20.32±0.98	3.33±0.30	23.36±0.73	0.860±0.01
MS-17B3	90	55.3	10.94±0.00	18.58±0.33	30.01±0.03	0.371±0.01
MS-18B3	90	50.4	14.44±0.05	19.72±0.05	33.66±0.02	0.423±0.01
MS-19B	90	50.7	21.66±0.60	9.80±0.90	31.84±0.66	0.689±0.02
MS-20B	90	45.5	19.71±0.46	22.53±0.40	42.48±0.71	0.467±0.01
MS-21B	90	45.9	22.54±0.58	16.37±0.15	38.95±0.94	0.579±0.01

Although there is good agreement between experiment and model for solutions $X_{NO3}<0.5$, there are discrepancies for both solution composition and relative humidity for nitrate-rich solutions near the eutonic. The model overpredicts relative humidity by as much as 8% relative humidity and underpredicts the solution composition by as much as 8 molal (or 40%). At 90 °C, the experimental data suggest a deliquescence relative humidity of 56% RH ($X_{NO3}=0.85$) compared

TABLE V. Solution % RH and composition from reversed deliquescence of NaCl–KNO_3 mixtures at 90 °C. Reported values represent the average steady-state solution composition.

Expt. ID	T (°C)	% RH ±3.1	Na molal	K molal	Cl molal	NO_3 molal	[Na]/ [Na]+[K]
			Initially dissolved salt				
MS-24A3	90	62.4	2.68±0.00	16.29±0.02	2.54±0.00	16.84±0.01	0.14±0.00
MS-25A4	90		6.07±0.01	6.56±0.04	5.82±0.01	6.58±0.01	0.48±0.01
MS-26A	90	55.3	4.75±0.14	15.36±0.20	4.71±0.08	15.95±0.30	0.24±0.01
MS-27A	90	54.7	7.07±0.34	11.97±1.04	5.80±0.08	13.64±1.49	0.37±0.01
MS-28A	90	65.5	1.55±0.11	18.09±0.04	1.63±0.06	18.07±0.05	0.08±0.01
MS-29A	90	65.3	5.71±0.09	3.71±0.23	5.79±0.05	3.74±0.22	0.61±0.01
MS-30A	90	71.5	5.43±0.00	0.42±0.07	5.53±0.01	0.44±0.06	0.93±0.01
MS-31A	90	52.4	5.96±0.25	15.85±0.39	5.06±0.09	16.74±0.40	0.27±0.00
MS-32A4	90	52.4	7.17±0.02	12.48±0.07	5.51±0.02	14.46±0.00	0.36±0.01
MS-35A4	90	56.4	6.61±0.07	9.90±0.03	5.93±0.00	10.29±0.05	0.40±0.01
MS-36A	90	51.5	6.98±0.43	16.68±0.38	5.35±0.06	17.91±0.05	0.29±0.02
MS-37A	90	50.7	8.00±0.06	14.91±0.07	5.56±0.04	17.59±0.12	0.35±0.00
			Initially solid salt				
MS-24B3	90	62.5	2.72±0.02	16.96±0.04	2.82±0.00	17.29±0.02	0.14±0.00
MS-25B4	90	62.8	6.22±0.01	6.61±0.06	5.89±0.04	6.68±0.01	0.48±0.01
MS-26B	90	55.6	4.99±0.05	15.40±0.37	4.93±0.04	16.08±0.22	0.24±0.00
MS-27B	90	55.7	7.17±0.40	12.48±1.45	5.73±0.09	14.11±1.91	0.37±0.01
MS-28B	90	65.7	1.64±0.09	18.10±0.20	1.82±0.09	18.08±0.21	0.08±0.00
MS-29B	90	65.6	5.81±0.02	4.09±0.21	5.80±0.01	4.08±0.23	0.59±0.01
MS-30B	90	71.9	5.54±0.02	1.03±0.04	5.60±0.02	1.05±0.03	0.84±0.00
MS-31B	90	52.7	6.57±0.16	16.04±0.04	5.34±0.11	17.28±0.07	0.29±0.00
MS-32B4	90	52.8	7.47±0.02	13.08±0.08	5.43±0.01	15.33±0.01	0.36±0.00
MS-35B4	90	55.8	6.91±0.06	10.57±0.07	5.60±0.02	11.54±0.02	0.40±0.01
MS-36B	90	50.9	7.53±0.20	16.50±0.22	5.52±0.11	18.18±0.28	0.31±0.00
MS-37B	90	51.1	8.06±0.07	15.12±0.11	5.58±0.05	17.70±0.18	0.35±0.00

TABLE VI. Solution % RH and composition from reversed deliquescence of NaCl–KNO_3 mixtures at 120 °C. Reported values represent the average steady-state solution composition.

Expt. ID	T (°C)	% RH ±3.1	Na molal	K molal	Cl molal	NO_3 molal	[Na]/ [Na]+[K]
Initially dissolved salt							
MS-34A(44)	120	43.0	8.35±0.00	17.19±0.32	6.14±0.00	20.22±0.05	0.33±0.01
MS-34A(41)	120	41.6	10.98±0.03	27.72±0.06	5.95±0.00	33.43±0.14	0.28±0.01
MS-34A(48)	120	48.1	8.18±0.06	16.55±0.25	6.09±0.02	19.27±0.06	0.33±0.01
MS-39A	119	47.3	9.14±0.07	20.33±0.13	6.09±0.04	23.85±0.09	0.31±0.01
MS-40A	119	47.9	5.54±0.05	30.26±0.08	5.53±0.00	30.38±0.13	0.16±0.00
MS-41A	119	45.7	9.86±0.05	22.09±0.03	6.22±0.02	26.44±0.06	0.31±0.01
MS-42A2	119	43.8	7.35±0.02	30.14±0.14	5.60±0.00	31.62±0.03	0.20±0.00
MS-43A2	119	43.3	10.65±0.03	24.90±0.04	6.00±0.03	29.29±0.17	0.30±0.00
MS-44A(40)	119	41.9	8.57±0.01	29.30±0.18	5.71±0.00	32.51±0.03	0.23±0.00
MS-44A(41)	119	42.9	8.19±0.01	29.28±0.09	5.45±0.00	31.94±0.05	0.22±0.00
Initially solid salt							
MS-33B(48)	120	48.7	4.64±0.03	27.60±0.22	4.60±0.03	27.94±0.03	0.14±0.00
MS-34B(44)	120	45.3	9.45±0.09	26.16±0.16	5.74±0.00	30.67±0.07	0.27±0.01
MS-34B(41)	120	41.0	10.89±0.03	28.53±0.11	5.92±0.00	34.26±0.06	0.28±0.01
MS-34B(48)	119	49.0	8.11±0.02	18.20±0.27	5.76±0.02	21.47±0.03	0.31±0.01
MS-38B	119	46.9	5.30±0.01	28.48±0.16	5.31±0.02	28.50±0.03	0.16±0.00
MS-39B	120	46.9	10.11±0.02	23.21±0.01	6.15±0.03	28.05±0.00	0.30±0.01
MS-40B	119	46.2	5.84±0.01	31.11±0.01	5.86±0.00	31.62±0.16	0.16±0.00
MS-41B	119	46.1	10.02±0.03	23.20±0.06	6.01±0.02	27.25±0.15	0.30±0.00
MS-42B2	119		7.37±0.01	31.58±0.16	5.83±0.00	33.11±0.01	0.19±0.00
MS-43B2	120	43.6	11.24±0.01	26.87±0.05	6.36±0.01	31.73±0.08	0.30±0.00
MS-44B(40)	119	41.3	9.11±0.05	28.91±0.31	5.69±0.01	32.42±0.02	0.24±0.00
MS-44B(41)	119	42.4	8.37±0.03	29.79±0.51	5.72±0.01	32.65±0.10	0.22±0.00

to the model prediction of 59% RH ($X_{NO3}=0.92$). Similarly at 110 °C, the experimental data suggest a deliquescence relative humidity of 52% RH ($X_{NO3}=0.9$) compared to the model prediction of 56% RH ($X_{NO3}=0.97$).

Although there are discrepancies in the absolute RH and solution composition, both experiment and model exhibit similar trends. Relative humidity decreases from a high value near 75% at low X_{NO3} to a minimum near the eutonic point. Above the eutonic point, the relative humidity increases with increasing X_{NO3} as the deliquescence point of pure soda niter is approached. The higher solubility of soda niter generates nitrate concentrations that are substantially higher than the chloride concentrations above $X_{NO3}=0.5$. Chloride concentrations decrease with increasing X_{NO3}, because chloride solubility is limited by the increasing sodium concentrations from dissolving soda niter (the common ion effect).

The solids consisted of halite with trace soda niter below the eutonic and of soda niter with trace halite above the eutonic. Trace amounts of soda niter and halite probably represent residual solution that was trapped in pore spaces during the filtration process when the salts were dried. Halite should be the only solid phase present below the eutonic because the solution is saturated with respect to halite and undersaturated with respect to soda niter. Above the eutonic, soda niter should be the only solid phase present, because the solution is saturated with respect to soda niter and undersaturated with respect to halite. Only at the eutonic, where both minerals are saturated, would one expect to find both halite and soda niter.

Figure 3 compares the experimental results of the reversed deliquescence experiments with the model calculations for the $KNO_3-NaNO_3-H_2O$ system at 90 °C. Similar to the NaCl–$NaNO_3-H_2O$ system, the convergence between the measured relative humidity and solution composition for initially dissolved and initially solid salt mixtures indicates that equilibrium was achieved. However, there is poor agreement between experiment and model for both the relative humidity and solution composition. Experimental relative humidity values are as much as eight percentage points higher than those predicted by the model on the niter side of the eutonic ($X_{Na}<0.2$). Trends in the experimental data indicate that the deliquescence relative humidity of about 42% agrees with the model prediction, but yields a more KNO_3 rich brine (about X_{Na} 0.5) than predicted by the model.

A large discrepancy between experiment and model is seen in the solution composition. Dissolved potassium, sodium, and nitrate concentrations follow similar trends as the model predictions, but the absolute concentrations are significantly higher. In the most extreme case, solution compositions are roughly twice the model prediction with experimental sodium=20 molal, potassium=22 molal, and nitrate=42 molal. The high experimental molal concentrations are not an artifact of deriving the values from solution analyses (see Sec. III D). A test of the analytical methodology using highly concentrated solutions showed that analytically and gravimetrically determined values were generally within 4% of each other. The solids consisted of niter with trace soda niter, below the experimental eutonic and of soda niter with trace niter, above the experimental eutonic. Trace amounts of soda niter or niter probably represent residual

solution that was trapped in pore spaces during the filtration process when the salts were dried.

Figures 4 and 5 compare the experimental results of the reversed deliquescence experiments with the model calculations for the $NaCl-KNO_3-H_2O$ system at 90 and 120 °C. Similar to the other salt systems studied here, the convergence between the measured relative humidity and solution composition for initially dissolved and initially solid salt mixtures indicates that equilibrium was achieved. Values for the deliquescence relative humidity are in agreement at both temperatures. This agreement at the eutonic relative humidity appears to be fortuitous, because there is poor agreement between experiment and model for relative humidity and all solution composition. The extent of the mismatch is much greater at 120 °C than at 90 °C. At 90 °C, the greatest mismatch occurs in KNO_3-rich solutions where the model underpredicts relative humidity by as much as five percentage points and underpredicts solution composition by as much as 4 molal (about 30%). In solutions dominated by NaCl ($X_{Na}>0.5$), there is reasonable agreement between model and experiment. At 120 °C, the mismatch between experiment and model relative humidity is similar to that at 90 °C. However, at this higher temperature, the model significantly underpredicts the solution composition. In the most extreme case, solution compositions are roughly twice the model prediction with experimental sodium=11 molal, potassium=28 molal, chloride=6 molal, and nitrate=33 molal. At 120 °C, atmospheric pressure limits the experiments to 50% relative humidity, so we cannot determine if the model adequately predicts relative humidity and solution composition in NaCl-rich solutions.

Analysis of the solids show that sylvite (KCl) is an important solubility control near the experimental eutonic in agreement with the results of model calculations at these temperatures. At 90 °C, niter, sylvite and minor amounts of halite were detected just to the left of the eutonic ($0.28 \leqslant X_{Na} \leqslant 0.31$), and halite, sylvite and minor amounts of niter were detected to the right side of the eutonic ($0.35 \leqslant X_{Na} \leqslant 0.40$). As is expected, the solids consisted of niter ($X_{Na} \leqslant 0.25$) and halite ($X_{Na} \geqslant 0.60$) on their respective limbs of the phase diagram. At 120 °C, solutions were saturated with repect to niter, sylvite, and halite between most of samples between $0.15 \leqslant X_{Na} \geqslant 0.30$. One sample at $X_{Na}=0.14$ contained only niter, two samples at $X_{Na}=0.16$ and $X_{Na}=0.30$ contained niter and halite, but no sylvite. Any trace amounts of salt detected probably represent residual solution that was trapped in pore spaces during the filtration process when the salts were dried.

V. DISCUSSION

A. Na–Cl, Na–NO_3, and K–NO_3 high-temperature Pitzer models

The comparison of model predictions and experimental results of relative humidity and solution compositions for the $NaCl-NaNO_3-H_2O$, $KNO_3-NaNO_3-H_2O$, and the $NaCl-KNO_3-H_2O$ systems from 90 to 120 °C indicate that some parameters used in the current high-temperature Pitzer model do not adequately describe brine chemistry formed by deliquescence of these salt mixtures. Before we discuss the specific data needs to resolve discrepancies between experimental results and model predictions, we review the basic high-temperature Pitzer model used in these simulations.[8]

The Pitzer model is derived by first defining an expression for the excess Gibbs free energy (G^{ex}) of the total solution [Ref. 9, Eq. (23)]:

$$\frac{G^{ex}}{RTw_w} = f(I) + \sum_i \sum_j \lambda_{ij}(I) n_i n_j + \sum_i \sum_j \sum_k \mu_{ijk} n_i n_j n_k, \quad (8)$$

where G^{ex} is the difference or "excess" in the Gibbs free energy between a real solution and an ideal solution defined on the molality composition scale, R is the universal gas constant, T is the absolute temperature, w_w is the mass (kg) of solvent water, f is a Debye–Hückel function that depends on the ionic strength ($I=1/2\Sigma_i m_i z_i^2$), λ_{ij} is a second-order interaction coefficient (also a function of I), μ_{ijk} is a third-order interaction coefficient, n denotes the number of moles of a species, and i, j, and k denote solute species. Here m denotes molality and z the charge number. Note that molality is defined as $m_i=n_i/w_w$. Upon substitution of $m_i w_w$ for n_i (and so forth for the j and k cases) in Eq. (8), the ionic solute activity coefficient (γ_i) and the solvent osmotic coefficient (ϕ) may be calculated as the partial derivatives with respect to the molality of the ionic solute and the mass of water, respectively:

$$\ln \gamma_i = [\partial(G^{ex}/w_w RT)/\partial m_i]_{n_w}, \quad (9)$$

$$\phi - 1 = -(\partial G^{ex}/\partial w_w)_{n_i}/RT\sum_i m_i \quad (10)$$

[Ref. 9, Eqs. (34) and (35)]. The activity of water is closely related to the osmotic coefficient ($\ln a_w = -(\Sigma_i m_i/\Omega)\varphi$, where Ω is the number of moles of water comprising a 1 kg mass, approximately 55.51).

Substitution of Eq. (8) into Eqs. (9) and (10) followed by differentiation yields the fundamental Pitzer equations for the solute activity coefficient and the osmotic coefficient (or alternative forms for the activity of water or the activity coefficient of water). See BSC[8] or Pitzer[9] for full details of the applied forms of the Pitzer equations and the corresponding practical interaction coefficients. Values for the practical interaction coefficients are generally obtained by fitting physical property measurements, such as the osmotic coefficient, the vapor pressure of water over salt solutions, or (less commonly) mineral solubilities.

The model requires only two-ion ($\beta^{(0)}_{MX}$, $\beta^{(1)}_{MX}$, $\beta^{(2)}_{MX}$, C^{ϕ}_{MX}, ${}^{S}\theta_{MM'}$ and ${}^{S}\theta_{XX'}$) and three-ion ($\psi_{MM'X}$ and $\psi_{MXX'}$) interaction parameters in the present study of ionic systems. Here M denotes a cation, M′ a different cation, X an anion, and X′ a different anion. The ${}^{S}\theta_{MM'}$, ${}^{S}\theta_{XX'}$, $\psi_{MM'X}$, and $\psi_{MXX'}$ parameters occur only in mixtures of aqueous electroltyes (e.g., MX–M′X, MX–MX′, or more complex mixtures). Within the framework of the standard Pitzer model, the values of the mixing parameters are independent of the possible presence of other types of ions in the solution, and

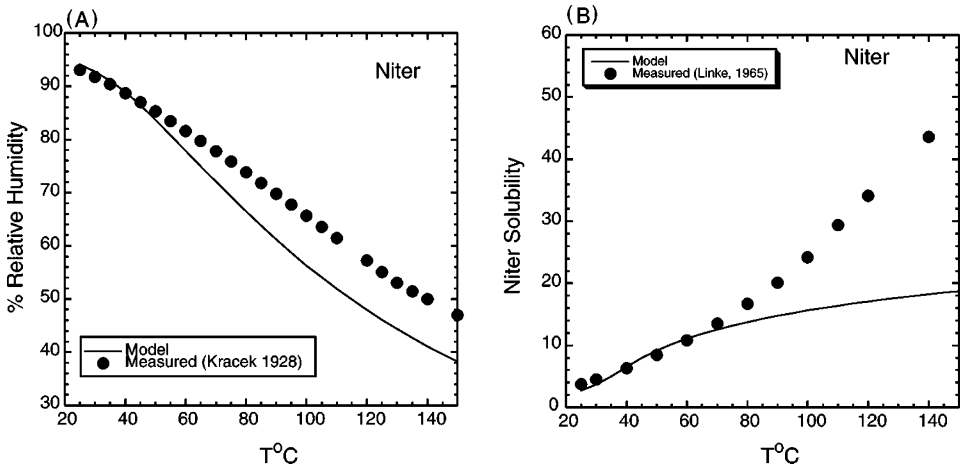

FIG. 7. Comparison of predicted and measured niter (KNO_3) (a) % relative humidity and (b) solubility as a function of temperature. Measured data are from Kracek[12] and Linke,[13] respectively. Predictions were made using EQ3/6 version 8 geochemical code and the Yucca Mountain high temperatured Pitzer ion interaction thermodynamic database (Refs. 6 and 8).

once their values have been determined for a particular system, the same values may be used for all other relevant systems.[9]

The high-temperature Pitzer model[8] employed in the present study uses the following equation to represent the temperature dependence of each of these ion interaction parameters:

$$\chi(T) = a_1 + \frac{a_2}{(T - T_r)} + a_3 \ln(T/T_r) + a_4(T - T_r), \qquad (11)$$

where χ represents any of the above-noted practical interaction parameters,[13] T_r is the reference temperature (298.15 K), and a_1, a_2, a_3, and a_4 are fitted coefficients. A variety of other forms are extant in the literature (e.g., Refs. 10, 14). For the model used here,[8] data taken from other models (see the following) were refit as necessary for consistency with the above temperature function. The differences associated with refitting from a different temperature function are negligible within the temperature ranges of the original fits.

Although the high-temperature Pitzer model used in the present study is a fairly comprehensive one accounting for the nonideal behavior of highly concentrated electrolytes over a wide range of temperature (nominally 0–200 °C), there are still significant data needs for common ions. The present model was founded on earlier high-temperature Pitzer models (Refs. 10, 14, and references cited by them), supplemented by parameter data from several other sources.[11,15–24] It is also partly based on refitting of parametrizations from the published literature to the most widely used (standard) form of the Pitzer equations.[25]

The Yucca Mountain Project high-temperature Pitzer model contains robust thermodynamic submodels for the $Na–NO_3$, Na–Cl, K–Cl, Na–K, and K–Na–Cl ion interactions. The $Na–NO_3$ model is based on data from −37 to 152 °C[11] that was refit for consistency with the standard Pitzer form. Some degradation in fit quality results from this refitting, increasing the deviation in the osmotic coefficient from about 0.01 to about 0.02.[25] Similarly, two-ion and three-ion models in the K–Na–Cl system are based on data from 0 to 300 °C[10] fit using the standard Pitzer form. In contrast, the $K–NO_3$ and $Cl–NO_3$ models are based on only 25 °C data[9] and there are no parameters for the $Na–K–NO_3$, $Na–Cl–NO_3$, or $K–Cl–NO_3$ ion interactions. Our experimental data in the $NaCl–NaNO_3–H_2O$ system indicate that temperature dependent parameters for $Cl–NO_3$ and/or $Na–Cl–NO_3$ ion interactions are needed to describe the relative humidity and the solution composition near the eutonic where maximum solubilities are approached. The absence of temperature dependent parameters for $K–NO_3$ ion interactions in the Yucca Mountain Project high-temperature Pitzer model is the primary cause of the poor prediction of the deliquescence of salt mixtures containing KNO_3 at elevated temperatures (Figs. 3–5) as well as the measured % relative humidity and solubility of KNO_3 at elevated temperature (Fig. 7). Additionally, some of the mismatch in the $NaCl–KNO_3–H_2O$ system may also be due to the absence of temperature dependent paramaters for $Cl–NO_3$, $Na–Cl–NO_3$, and/or $K–Cl–NO_3$ ion interactions, in addition to the absence of temperature dependent $K–NO_3$ ion interaction parameters.

B. Implications for radioactive waste disposal

It is important that geochemical calculations of the chemical environment at the waste package surfaces use a robust high-temperature Pitzer ion interaction model for common ions, because the deliquescence of aerosol salts and dust is likely to be a primary source of brines that contact the waste containers and drip shields. In addition to the discrepancy identified for relative humidity and solution composition for salt mixtures containing KNO_3 stemming from the use of a constant temperature model for $K–NO_3$ interactions, discrepancies for magnesium and ammonium salt mixtures at elevated temperatures are likely because the model includes constant temperature models for many of their respective ion interactions.[8] Osmotic and activity coefficients must be experimentally determined as a function of temperature to derive the ion interaction parameters needed to describe the nonideal behavior of these concentrated solutions, because the Pitzer model is empirically based. Of the salt systems listed above, robust models for potassium salts are probably the most important at high temperature, because magnesium

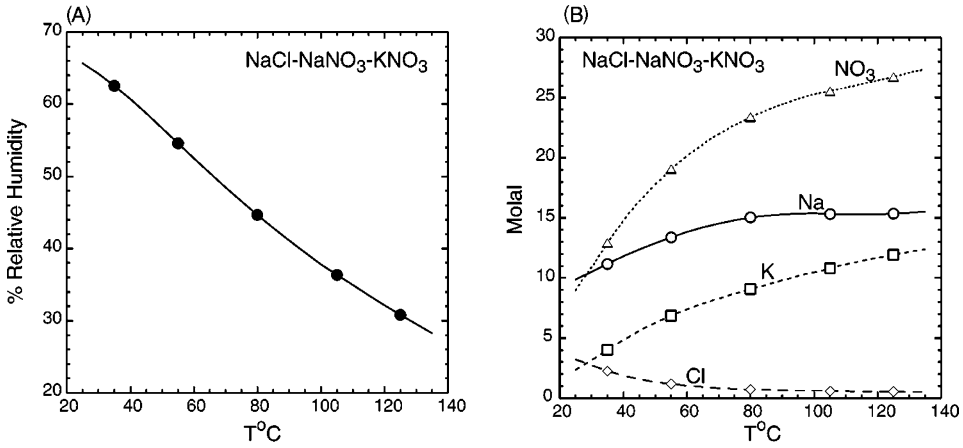

FIG. 8. Model predictions of brine (a) % relative humidity and (b) solution composition as a function of temperature at the deliquescence point for a $NaCl–NaNO_3–KNO_3$ mineral assemblage (Ref. 8). Predictions were made with EQ3/6 geochemical code and the high temperature Pitzer ion interaction thermodynamic data base. Triangles, circles, squares, and diamonds represent NO_3, Na, K, and Cl concentrations.

concentrations are likely to be limited by insoluble silicate minerals[26] and ammonium concentrations are likely to be limited by gas volatility.

Recent modeling efforts by the Yucca Mountain Project predict that mixtures of NaCl, KNO_3 and/or $NaNO_3$ are the most prevalent mineral assemblages that may deliquesce in repository environments using the current high-temperature Pitzer model.[8] As the temperature increases, the deliquescence relative humidity and the NO_3 concentrations increase (Fig. 7). We expect only small differences between predicted and actual deliquescence relative humidity and brine composition at temperatures below 60 °C, because the model adequately predicts niter solubility at these temperatures. However, at higher temperatures, much larger differences between predicted and actual environment are expected, because the model underpredicts niter solubility by about 200% at 135 °C [Fig. 7(b)]. At these temperatures the current Pitzer model will significantly underpredict brine NO_3 brine composition because the $K–NO_3$ interactions will be more important. This is clearly illustrated in our $KNO_3–NaNO_3$ and $NaCl–KNO_3$ deliquescence experiments, where NO_3 concentrations can be twice the predicted concentrations. Additionally, it is likely that calculated deliquescence relative humidities for the three salt system are of limited accuracy, because the current model for KNO_3 is of limited accuracy at high temperature (Fig. 8). Therefore calculated dry-out or deliquescence temperatures are uncertain. Dry-out or deliquescence temperatures made assuming a total pressure similar to current atmospheric pressure (0.90 bar) predict that a brine saturated with NaCl, $NaNO_3$, and KNO_3 would boil just above 135 °C.[6]

VI. CONCLUSIONS

Adsorption of water by deliquescent salt minerals found in aerosols and dusts that may be deposited on waste package surfaces during the construction and ventilation stages of a high-level radioactive waste repository at Yucca Mountain, NV, will be a primary source of brines that might lead to corrosion of the waste package surfaces. Although the deliquescence relative humidity of most pure salt minerals is known over a range of temperature, the behavior of salt mixtures at elevated temperatures is unknown. Our reversed deliquescent experimental results in saturated $NaCl–NaNO_3–H_2O$, $KNO_3–NaNO_3–H_2O$, and $NaCl–KNO_3–H_2O$ systems from 90 to 120 °C show that use of 25 °C parameter values for $K–NO_3$ and $Cl–NO_3$ (and possibly for three-ion parameters in the $Na–K–Cl–NO_3$ system) in the Yucca Mountain Project high-temperature Pitzer model do not accurately predict the equilibrium solubility and corresponding relative humidity of KNO_3 salt mixtures and of $NaCl–NaNO_3$ mixtures near the eutonic composition.

ACKNOWLEDGMENTS

We thank Greg Gdowski, Joe Rard, Maureen Alai, and Que Anh Nguyen for their contributions to the experiments. This work was performed under the auspices of the U.S. Department of Energy by the University of California, Lawrence Livermore National Laboratory under Contract No. W-7405-Eng-48.

[1] G. M. Gordon, Corrosion **58**, 811 (2002).
[2] L. Greenspan, J. Res. Natl. Bur. Stand., Sect. A **81**, 89 (1977).
[3] Z. Ge, A. S. Wexler, and M. V. Johnston, J. Phys. Chem. A **102**, 173 (1998).
[4] I. N. Tang and H. R. Munkelwitz, Atmos. Environ., Part A **27A**, 467 (1993).
[5] I. N. Tang and H. R. Munkelwitz, J. Appl. Meteorol. **33**, 791 (1994).
[6] BSC (Bechtel SAIC Company), ANL-EBS-MD-000001 REV 01, Las Vegas, Nevada, 2004.
[7] T. J. Wolery and R. L. Jarek, 2003. EQ3/6, Version 8.0, Software User's Manual, Software Document Number: 10813-UM-8.0-00, U.S. Department of Energy, Office of Civilian Radioactive Waste Management, Office of Repository Development, 1261 Town Center Drive, Las Vegas, NV 89144.
[8] BSC (Bechtel SAIC Company), in ANL-EBS-MD-000045 REV 02. Las Vegas, NV, Bechtel SAIC Company, 2004b.
[9] K. S. Pitzer, in *Activity Coefficients in Electrolyte Solutions*, 2nd. ed., edited by K. S. Pitzer (CRC Press, Boca Raton, FL, 1991), pp. 75–153.
[10] J. P. Greenberg and N. Møller, Geochim. Cosmochim. Acta **53**, 2503 (1989).
[11] D. G. Archer, J. Phys. Chem. Ref. Data **29**, 1141 (2000).
[12] F. C. Kracek, in *International Critical Tables of Numerical Data, Physics, Chemistry and Technology*, edited by E. Washburn (1928), Vol. 3, pp. 351–374.
[13] W. F. Linke, *Solubilities: Inorganic and Metal-Organic Compounds. V. 2, K-Z.*, 4th ed. (American Chemical Society, Washington, DC, 1965), p. 200.
[14] N. Møller, Geochim. Cosmochim. Acta **52**, 821 (1988).
[15] H. F. Holmes, R. H. Busey, J. M. Simonson, and R. E. Mesmer, J. Chem. Thermodyn. **19**, 863 (1987).
[16] R. T. Pabalan and K. S. Pitzer, Geochim. Cosmochim. Acta **51**, 2429 (1987).

[17] S. L. Clegg and P. Brimblecombe, J. Phys. Chem. **94**, 5369 (1990a).
[18] S. L. Clegg and P. Brimblecombe, Geochim. Cosmochim. Acta **54**, 3315 (1990b).
[19] W. E. Thiessen and J. M. Simonson, J. Phys. Chem. **94**, 7794 (1990).
[20] S. He and J. W. Morse, Geochim. Cosmochim. Acta **57**, 3533 (1993).
[21] A. R. Felmy, C. C. Schroeder, and M. J. Mason, PNL-SA-25345, Pacific Northwest National laboratory, Richland, WA, 1994.
[22] S. L. Clegg, S. Milioto, and D. A. Palmer, J. Chem. Eng. Data **41**, 455 (1996).
[23] H. F. Holmes and R. E. Mesmer, J. Chem. Thermodyn. **30**, 723 (1998).
[24] C. S. Oakes, A. R. Felmy, and S. M. Sterner, J. Chem. Thermodyn. **32**, 29 (2000).
[25] J. A. Rard and A. M. Wijesinghe, J. Chem. Thermodyn. **35**, 439 (2003).
[26] M. Alai, M. Sutton, and S. Carroll, Geochem. Trans. (submitted).